Malaysian Journal of Analytical Sciences (MJAS)
Published by Malaysian Analytical Sciences Society

POTENTIAL OF TEXTILE WASTE AS NITROGEN DOPED POROUS CARBON FOR OXYGEN REDUCTION REACTION

(Potensi Sisa Tekstil Sebagai Karbon Poros Terdop Nitrogen Berliang untuk Tindak Balas Penurunan Oksigen)

Suhaila Mohd Sauid[1, 3], Siti Kartom Kamarudin[1,2]*, Loh Kee Shyuan[1]

[1]*Fuel Cell Institute*
[2]*Department of Chemical and Process Engineering, Faculty of Engineering and Built Environment*
Universiti Kebangsaan Malaysia, 43600 UKM Bangi, Selangor, Malaysia
[3]*School of Chemical Engineering, College of Engineering*
Universiti Teknologi MARA, 40450 Shah Alam, Selangor, Malaysia

**Corresponding author: ctie@ukm.edu.my*

Received: 13 December 2021; Accepted: 27 February 2022; Published: 27 June 2022

Abstract

Transforming waste into usable materials can protect and conserve the environment, thereby reducing the dependence on landfills, limiting the use of natural resources, and decreasing the carbon footprint. Every year, millions of tons of textile waste are sent to landfills primarily from discarded clothing. Therefore, this waste is worthwhile to convert into functional carbon product. Herein, textile waste from used clothing was converted into nitrogen-doped porous carbons (TNPC) by simple chemical activation followed by carbonisation. Urea and calcium chloride ($CaCl_2$) served as nitrogen precursor and pore forming agent, respectively. The surface area and porosity of the prepared TNPCs were affected by the activation temperature. The optimal sample (TNPC900) activated at 900 °C exhibited a large surface area (496 m^2 g^{-1}) with appropriate porosity and a reasonable amount of nitrogen doped. Remarkably, the resultant TNPC900 catalyst tested as the electrode material for oxygen reduction reaction in 0.1 M KOH exhibited an outstanding positive onset potential of 0.94 V vs. RHE. TNCP900 catalyst also demonstrated superior stability and tolerance to methanol than Pt/C. Overall, this study showed that the conversion of textile waste through a simple synthesis technique into electrocatalyst could offer a sustainable alternative to Pt for potential applications in fuel cell and energy-storage technology.

Keywords: textile waste, nitrogen-doped porous carbon, oxygen reduction reaction, metal-free catalyst

Abstrak

Mengubah sisa menjadi bahan yang boleh digunakan dapat melindungi dan memulihara alam sekitar sekaligus dapat mengurangkan kebergantungan pada tapak pelupusan sampah, mengehadkan penggunaan sumber semula jadi, dan mengurangkan jejak karbon. Setiap tahun, jutaan ton sisa tekstil dihantar ke tapak pelupusan sampah terutama dari pakaian terpakai. Oleh itu, menukar sisa ini menjadi produk karbon berfungsi adalah usaha yang berbaloi. Di sini, sisa tekstil daripada pakaian terpakai telah ditukar kepada karbon berliang terdop nitrogen (TNPC) dengan pengaktifan kimia mudah diikuti dengan langkah karbonisasi. Urea dan kalsium klorida ($CaCl_2$) bertindak masing-masing sebagai bahan sumber nitrogen dan ejen pembentukan liang. Keluasan permukaan dan keliangan TNPC yang disediakan telah dipengaruhi oleh suhu pengaktifan.

Sampel optimum (TNPC900) diaktifkan pada 900 ° C mempamerkan keluasan permukaan yang besar (496 m^2 g^{-1}) dengan keliangan dan jumlah nitrogen terdop yang sesuai. Mangkin TNPC900 yang diuji sebagai bahan elektrod untuk tindak balas penurunan oksigen (ORR) di dalam larutan 0.1 M KOH menunjukkan potensi permulaan positif yang luar biasa iaitu 0.94 V vs RHE. Selain itu, mangkin TNCP900 menunjukkan kestabilan dan toleransi yang unggul terhadap metanol daripada mangkin Pt/C. Oleh itu, kajian ini menunjukkan bahawa penukaran sisa tekstil menggunakan teknik sintesis yang mudah menjadi elektmangkin dapat menawarkan alternatif Pt yang mampan untuk aplikasi di dalam sel bahan api dan teknologi penyimpanan tenaga.

Kata kunci: sisa tekstil, karbon poros terdop nitrogen, tindak balas penurunan oksigen, mangkin bebas metal

Introduction

The growing demand of green and efficient energy has driven the exploration for new technologies because of the depletion of fossil fuels and major environmental problems associated with the usage of conventional energy sources. Fuel cells are a competitive energy device for supplying energy with promising efficiency and negligible emission levels through electrochemical reactions into electricity [1]. However, the sluggish oxygen reduction reaction (ORR) at the cathode significantly affects the overall fuel-cell performance and thus requires an efficient catalyst to accelerate the ORR. The scarce platinum (Pt) and its alloy are extensively used as ORR catalysts, but their high price, low stability, and susceptibility to methanol crossover hinder its large-scale application [2, 3]. Extensive researches have been performed for Pt alternatives that are more cost effective and sustainable with high ORR activity [4]. Metal-free nitrogen-doped carbon materials exhibit massive potential as a substitute to costly Pt-based catalysts, where it demonstrates good ORR electrocatalytic activity and durability, even in acidic electrolytes [5, 6]. Furthermore, owing to the absence of metals, these catalysts could significantly reduce the cathode cost [7].

In recent years, biomass-derived nitrogen-doped carbon materials have prompted fascination and huge consideration in various energy-related applications [8]. Since 2010, many types of biomass such as animal and plant biomass, starch, cellulose derivatives, sugar, microorganisms such as fungi and yeast, and human and industrial waste have been converted into nitrogen-doped carbon for ORR [9, 10]. Biomass materials are used because of their adequate source of carbon, relatively low cost, readily available around the world, and environment friendliness [11, 12]. In particular, the transformation of waste biomass into nitrogen-doped carbon materials reduces the use of natural resources and thus lowers the carbon footprint, eventually leading to less dependence on landfills. Over the past 15 years, the manufacture and use of textile have increased twofold owing to cheaper production cost, more efficient operation, and increasing demand caused by the fast changing fashion industry [13]. Inevitably, more textile waste is created when more textiles are produced. In the U.S only, 11.3 million tonnes of textiles are disposed in landfills, and only 14.7% (2.5 million tonnes) of the total textiles waste generated is being recycled [14]. The reason for the small amount of textiles being recycled is the complexity of segregating the blended fabric materials [15]. Therefore, the conversion of textiles waste into other usable novel materials is worth exploring.

In the present work, we developed metal-free nitrogen-doped porous carbon for ORR from discarded clothing. Urea and calcium chloride were used as nitrogen source and pore-forming agent, respectively, during synthesis. Different pyrolysis temperatures were used to explore temperature's effect on the surface characteristics and electrochemical performance of the electrocatalyst. The obtained nitrogen-doped carbon showed a comparable electrocatalytic activity to that of Pt/C, with superior stability and tolerance to methanol.

Materials and Methods

Preparation of nitrogen-doped porous carbon

TNPCs were fabricated following a previously reported procedure [16]. Typically, small textile cuts of polyester blend fabrics were impregnated in solution containing calcium chloride and urea for 12 h. Then, it

was dried at 80 °C for another 12 h prior to pyrolysis at the desired temperature (800, 900, and 1000 °C) for 1 h in N_2 environment. After cooling to room temperature, the pyrolysis products were ground using pestle and mortar into fine powder and then acid etched in 3 M HCl to remove any unstable elements. Multiple rinsing with distilled water was conducted until the eluent reached neutral pH before finally drying at 105 °C overnight. The prepared sample was denoted according to its pyrolysis temperature, i.e., TNPC800, TNPC900, and TNPC1000 for 800, 900, and 1000 °C, respectively.

Surface characterisation

The surface morphology of the TNPCs was examined by scanning electron microscopy (SEM; CARL ZEISS EVO MA 10). The Brunauer–Emmett–Teller (BET) surface area and porosity of TNPCs were determined from nitrogen adsorption–desorption isotherms evaluated by a Micromeritics 3 Flex instrument. The surface element and binding energy of the prepared TNPCs were analysed by X-ray photoelectron spectroscopy (XPS) by using an Axis Ultra DLD system (Kratos) with a monochromic Al/K-Alpha X-ray source. Background correction were performed for all peaks with carbon peaks (284.8 eV).

Electrochemical characterisation

Electrochemical tests were performed using an Autolab PGSTAT128N potentiostat (Metrohm-Autolab) with a rotating ring-disk electrode (RRDE). A typical three-electrode system comprising a platinum rod, 5 mm-diameter glassy carbon, and Ag/AgCl electrodes serving as counter, working, and reference electrodes, respectively, were used. The catalyst ink was prepared by dispersing 4 mg of catalyst powder in the mixture of deionised water, ethanol, and 5wt% Nafion solution. ORR measurements were conducted by cyclic voltammetry (CV) in N_2- and O_2-saturated 0.1 M KOH solution at a scan rate of 25 mV s^{-1}, whereas linear scan voltammetry (LSV) was performed at a sweeping rate of 5 mV s^{-1} from 100 to 1600 rotation speeds. CV and LSV were swept within the same potential range from 0.2 V to -0.9 V vs. Ag/AgCl. For comparison, 20wt% Pt/C with the same catalyst loading was used in the electrochemical measurement. Kinetic current density (j_K) was calculated according to equation (1) where j, j_K, and j_L are the measured, kinetic current, and the diffusion-limiting current densities, respectively.

$$j_K = \frac{j \cdot j_L}{j_L - j} \quad (1)$$

The electron-transfer number (n) was calculated from the Koutecky–Levich (K-L) equations (2) [17].

$$\frac{1}{j} = \frac{1}{j_K} + \frac{1}{j_L} = \frac{1}{B}\omega^{-1/2} + \frac{1}{j_K} \quad (2)$$

where ω is defined as the angular velocity (rad s^{-1}), and the proportionality coefficient B is defined as equation (3) [17].

$$B = 0.62D^{2/3}\nu^{-1/6}nFC^{*} \quad (3)$$

where D is the diffusion coefficient of O_2 in 0.1 M KOH (1.9×10^{-5} cm^2 s^{-1}), ν is the kinematic viscosity of the electrolyte (0.01 cm^2 s^{-1}), F is the Faraday constant (96485C mol^{-1}), and C^* is the concentration of O_2 in 0.1 M KOH (1.2×10^{-6} mol cm^{-3}) [18]. Electron-transfer numbers (n) and H_2O_2 (%) yield were calculated from the RRDE curves using equations (4) and (5), respectively [19].

$$n_{RRDE} = 4 \times \frac{i_d}{i_d + i_r/N_c} \quad (4)$$

$$H_2O_2\ (\%) = 200 \times \frac{i_r/N_C}{i_d + i_r/N_c} \quad (5)$$

where i_r is the ring current, i_d is the disk current, and N_c is the disk-current collection efficiency of ring electrode. (N_c= 0.256). For stability test, we compared the LSV curves of before and after a continuous 1000 CV cycle of 100 mV s^{-1} scan rate in O_2-saturated 0.1 M KOH of TNPC and Pt/C. The ring potential was set at 1.4 V vs. RHE during the RRDE measurement, which was within the recommended potential window of inducing H_2O_2 oxidation to O_2 [17].

Results and Discussion

Surface characterisation of TNPCs

The SEM images of TNPC800, TNPC900, and TNPC1000 are shown in Figure 1, respectively. All three samples had pore-like morphology on the TNPC surface. For TNPC800 and TNPC900, the pores were

more visible and had depth (Figures 1a and 1b, respectively), whereas the pores on TNPC1000 were larger and seemed shallower as if the pores had collapsed (Figure 1c). This finding indicated that the development of pore structures on TNPCs was affected by pyrolysis temperature. An electrocatalyst with porous structure is desirable as it could accommodate abundant active sites and transport channels for ions [20, 21].

N_2 adsorption–desorption isotherm was used to determine the porosity properties of the TNPC samples. As shown in Figure 1(d), all TNPCs demonstrated type-IV isotherm curves with a clear hysteresis loop (parallel adsorption and desorption branches) at $P/P_o \approx 0.45–1.0$, signifying the existence of mesopores in all samples [22]. Furthermore, the BJH pore-size distribution plot (Figure 1d inset) also confirmed that all samples contained mesopores within their distribution. The surface areas calculated based on BET for all TNPCs are listed in Table 1. TNPC900 had the largest surface area of 495.97 m^2 g^{-1} and the highest pore volume within the range of the pyrolysis temperature studied. Furthermore, the surface area increased with increased temperature from 800 °C to 900 °C but significantly dropped when the pyrolysis temperature was 1000 °C with decreased surface area to 207.76 m^2 g^{-1}. The pore volume also followed the same trend as the surface area. However, the ratio of S_{meso}/S_{micro} increased with increased pyrolysis temperature. This finding indicated that with increased temperature to 1000 °C, the micropore structures collapsed and created larger pores. Consequently, the surface area decreased, as supported by the higher average pore size obtained at 1000 °C. The increase in pore diameter well agreed with the morphology observed by SEM. Given that ORR occurs at the interfacial/surface of a catalyst, the micro- and mesoporous structure of a catalyst with high surface area and pore volume can serve as abundant active sites influencing the mass-transport properties and diffusion of the electrolyte [23, 24]. Therefore, the porosity structure of these TNPCs is expected to affect ORR performance.

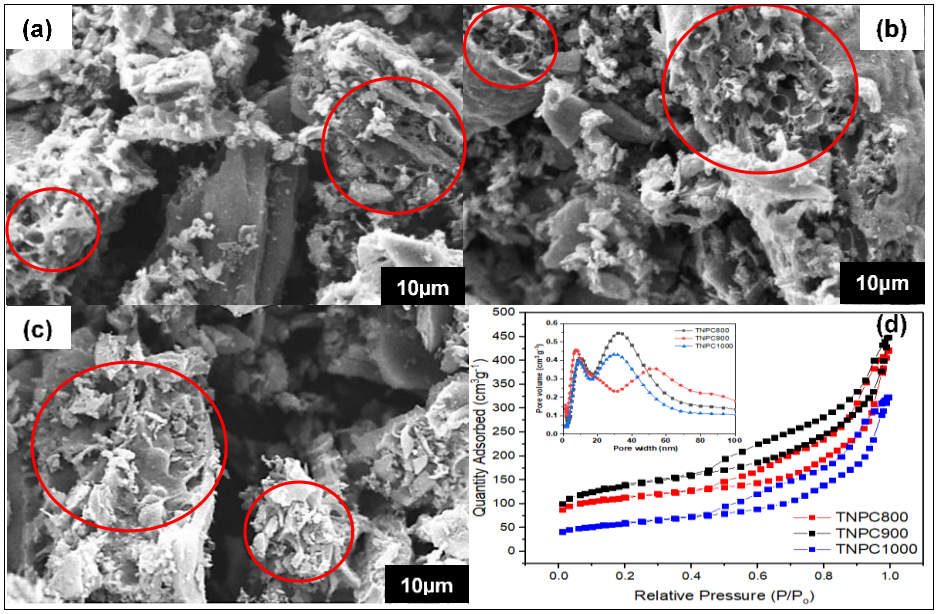

Figure 1. SEM images of (a) TNPC800, (b) TNPC900, (c) TNPC1000 (1k magnification respectively), and (d) N_2 adsorption–desorption isotherms of TNPCs (inset, corresponding pore-size distribution)

N_2 adsorption-desorption isotherm was used to determine the porosity properties of the TNPC samples. As shown in Figure 1 (d), all TNPCs demonstrate type IV isotherm curves with a clear hysteresis loop (parallel adsorption and desorption branches) at P/P_o ~0.45 – 1.0, signify the existence of mesopores in all samples [22]. Furthermore, the BJH pore size distribution plot (Figure 1d inset) also corroborates that all samples contain mesopores within their distribution. The surface area calculated based on Brunauer-Emmett-Teller (BET) for all TNPCs are tabulated in Table 1. As we can see, TNPC900 has the largest surface area of 495.97 m^2 g^{-1} and the highest pore volume in the range of the pyrolysis temperature studied. Furthermore, the surface area enlarge as the temperature was increased from 800 to 900 °C but drop significantly when the temperature of pyrolysis was at 1000 °C as the surface area reduced to 207.76 m^2 g^{-1}. The pore volume also follows the same trend as surface area. However, the ratio of S_{meso}/S_{micro} increase with the increment in pyrolysis temperature. This might indicate that as the temperature raised to 1000 °C, the micropore structures had collapsed which creating larger pores thus decreasing the surface area and this is supported by the higher average pore size obtained at 1000 °C. The increase in pore diameter is in agreement with the morphology observed by SEM. Since ORR occur at the interfacial/surface of a catalyst, the micro- and mesoporous structure of a catalyst with high surface area and pore volume can serve as abundance active sites that influence the mass transport properties and diffusion of the electrolyte [23,24]. Therefore, it is expected that the porosity structure of these TNPCs will affect the ORR performance.

Table 1. Surface properties of TNPCs

Sample	S_{BET} (m^2 g^{-1})	S_{micro} (m^2 g^{-1})	S_{meso} (m^2 g^{-1})	S_{meso} / S_{micro} ratio	Pore Volume (cm^3 g^{-1})	Average Pore Size (nm)	C (at%)	N (at%)	O (at%)
TNPC800	416.1	235.55	180.55	0.43	0.64	6.12	92.96	3.54	2.88
TNPC900	495.97	214.77	281.20	0.57	0.67	5.43	91.85	2.80	3.99
TNPC1000	207.76	54.36	153.40	0.74	0.49	9.43	93.39	1.54	3.86

The surface compositions and bonding states of all samples were analysed by XPS. Figure 2(a) displays the survey scans of TNPC samples. C 1s, N 1s, and O 1s were identified at binding energies around 284, 400, and 532 eV. The presence of a small N 1s signal indicated that nitrogen was successfully doped into carbon. The estimated elemental content is listed in Table 1. The nitrogen content can be as high 3.54 at% for TNPC800 and as low as 1.54 at% for TNPC1000, indicating that increased temperature significantly affected nitrogen doping. High-resolution scans of N 1s were further performed to investigate its chemical structure and deconvoluted into three peaks, as exemplified in Figure 2(b). The peaks at 398.4, 400.0, and 401.5 eV corresponded with pyridinic-N, pyrrolic-N, and graphitic-N, respectively [25, 26]. Pyridinic-N is when two carbon atoms located at the edge of graphitic planes are bound to the nitrogen atom, whereas pyrrolic-N is the nitrogen atom incorporated into the pentagonal ring. Meanwhile, graphitic-N is when a nitrogen atom replaces a carbon atom and bonded with three carbon atoms in the graphene layer [27, 28]. As shown in Figure 2(c), pyridinic-N was the highest for TNPC900 followed by TNPC1000. Furthermore, the rise in temperature from 900 °C to 1000 °C reduced the contents of pyridinic-N slightly but significantly reduced pyrrolic-N. By contrast, the graphitic-N content rose to almost 50 at% at 1000 °C, which was attributed to the transformation of pyrrolic-N and fractional conversion of pyridinic-N into

graphitic-N from the condensation of graphite rings at 1000 °C [29]. Recent studies have reported that pyridinic-N and graphitic-N played important roles in enhancing ORR performance [30, 31]. Pyridinic-N provided active sites and facilitated the dominant 2e⁻ to 4e⁻ process in the ORR mechanism, whereas graphitic-N promoted the reduction of oxygen to hydrogen peroxide by adsorbing OOH intermediates through a 2e- pathway [32].

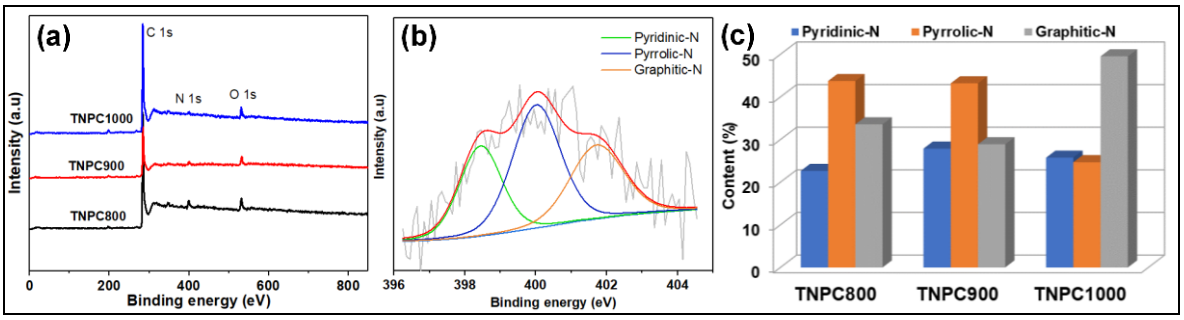

Figure 2. (a) XPS survey spectra; (b) high-resolution XPS of N 1s for TNPC900, and (c) content of nitrogen species of TNPC800, TNPC900, and TNPC1000

Electrochemical performance of TNPCs

To investigate the possible application of the prepared catalysts for fuel-cell or energy-storage systems, the electrochemical activity of TNPCs was evaluated using a three-electrode system. RRDE or a glassy carbon electrode was loaded with the as-prepared catalyst ink with 0.285 mg cm^{-2} loading. As shown in Figure 3 (a), all three catalysts showed no reduction peak observed in N_2-saturated 0.1 M KOH solution but obvious peaks in a solution of O_2 saturated with the same electrolyte, indicating that these TNPCs were catalytically active towards ORR. However, TNPC900 illustrated a stronger cathodic peak at 0.76 V vs. RHE, and it was more positive than TNPC800 and TNPC1000. Figure 3(b) shows the LSV plots for TNPCs and the commercial Pt/C (20wt%) at 1600 rpm in O_2-saturated electrolyte. Amongst the three TNPCs, TNPC900 had the highest ORR activity based on the most positive onset potential E_o and half-wave potential $E_{1/2}$ at 0.94 and 0.78 V vs. RHE, respectively. The E_o and $E_{1/2}$ of TNPC800 (0.92 and 0.74 V, respectively) and TNPC1000 (0.93 and 0.75 V, respectively) were more negative than those of TNPC900. The E_o of TNPC900 was slightly inferior to that of commercial Pt/C but comparable with values obtained in previous studies using a different biomass, such as coconut mesocarp [26], but higher than those of waste lotus seedpod [12] and cotton stalk [33]. The ORR activity of the TNPCs can also be assessed by their kinetic current densities (j_K) [34]. The j_K values at 0.8 V vs. RHE were in the order TNPC900 (1.82 mA cm^{-2}) > TNPC1000 (0.55 mA cm^{-2}) > TNPC800 (0.46 mA cm^{-2}), consistent with E_o and $E_{1/2}$.

To further investigate the kinetic information of ORR for TNPC900, LSV curves were collected at different rotating speeds from 100 rpm to 1600 rpm in O_2-saturated 0.1 M KOH solution (Figure 3(c)). With increased rotation, the limiting current density increased because of the shorter distance of diffusion [12]. The K-L plot (Figure 3(c) inset) illustrated a linear trend for the potential range of 0.2 V to 0.6 V vs. RHE, signifying similar electron-transfer number (3.5–3.8) around these potentials. The corresponding electron-transfer number calculated from the ring current and disk current of RRDE (3.55–3.73) curve also agreed with the K-L results (Figure 3d) suggesting a dominant 4e⁻ pathway in ORR for TNPC900 catalyst. Conversely, the electron-transfer number calculated for TNPC800 (3.35–3.53) and TNPC1000 (3.48–3.58) was slightly lower than that for TNPC900, indicating that ORR occurred through a combined 2e⁻ and 4e⁻ transfer pathway. The yield of H_2O_2 shown in Fig. 3d indicated lesser H_2O_2 formation on TNPC900, further validating

a higher catalytic efficiency of TNPC900 in 0.1 M KOH solution.

The superior ORR performance of TNPC900 may be largely influenced by the highest surface area, proper ratio of mesopores over micropores, and the role of pyridinic-N. Given that pyridinic-N served as the active sites for the adsorption and dissociation of oxygen [35], TNPC900 exhibited superior ORR activities than the other TNPCs. However, despite TNPC800 having a slightly lower surface area than TNPC900 and the highest nitrogen content (Table 1), its effect was not as important to ORR as the E_o and $E_{1/2}$ were the lowest for TNPC800. This finding may be due to the higher proportion of micropores (56.6%) dominating the effect to ORR because the restricted active sites such as micropores were difficult to be wet by liquid electrolyte [36]. This finding was further supported by the higher ORR characteristics of TNPC1000 that even though the surface area and the nitrogen content were the least (Table 1), the larger proportion of mesopores was assumed to facilitate a better ORR activity than TNPC800.

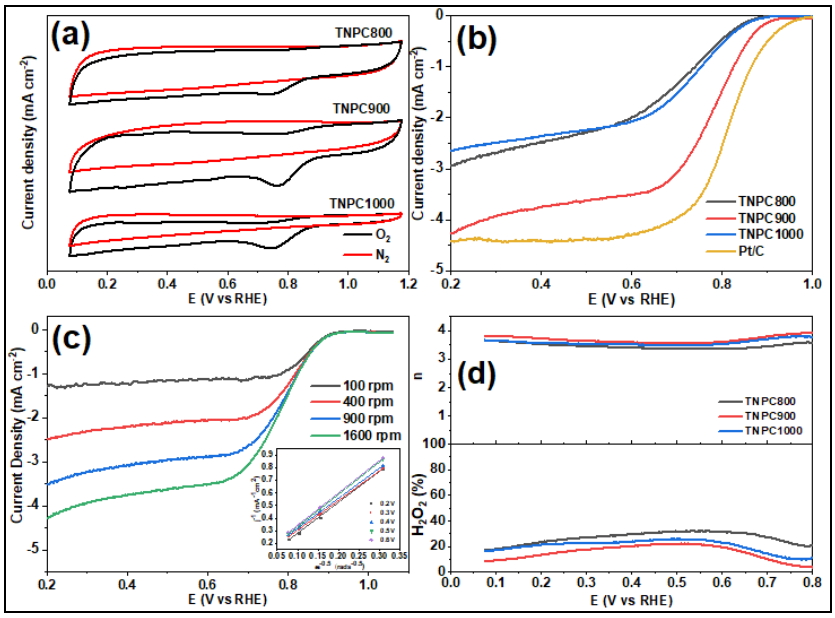

Figure 3. (a) CV curves of TNPCs in N_2- or O_2-saturated 0.1 M KOH solution. (b) LSV of samples and Pt/C. (c) LSV of TNPC900 at different rotation speeds (inset, K-L plots of TNPC at 0.2 V to 0.6 V vs. RHE). (d) Plots of number of electron transfer; n and H_2O_2 yield of TNPC900 calculated from RRDE currents

Stability of TNPC900

To evaluate the durability of TNPC900, stability test particularly CV was performed in O_2-saturated 0.1 M KOH at a scan rate of 100 mV s^{-1}. After 1000 potential cycles, the E_o and $E_{1/2}$ of TNPC900 remained unchanged (Figure 4a), whereas a significant negative shift was observed for Pt/C (Figure 4(a) inset) under the same condition. Pt/C also experienced 11% loss of the limiting current density. These results indicated TNPC900 had a relatively better stability than Pt/C under alkaline condition. TNPC900 also showed good tolerance to methanol (Figure 4(b)) as the CV curve was similar before and after adding 3 M methanol. Conversely, a visible oxidation peak emerged for Pt/C (Figure 4(b) inset), which was typical owing to the higher selectivity of Pt for methanol oxidation reaction than ORR [37]. Therefore, the superior stability and methanol tolerance of TNPC900 over Pt/C signified possible application in direct methanol fuel-cell application.

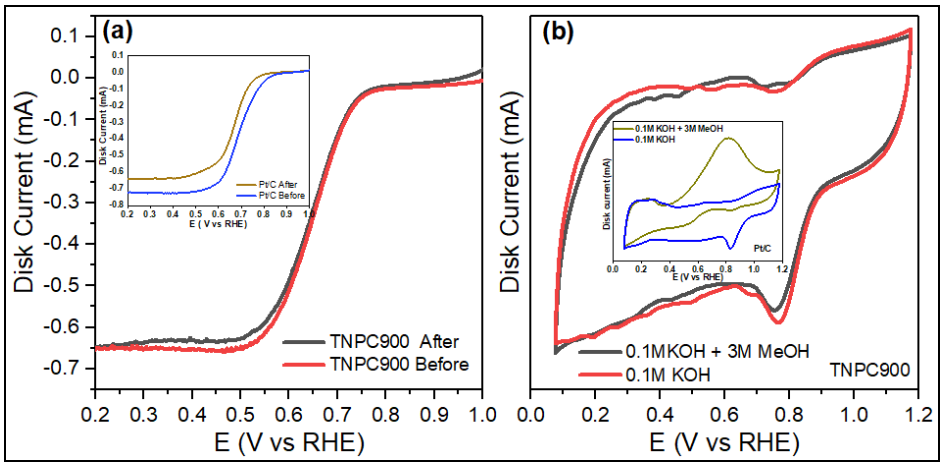

Figure 4. (a) LSV plots for TNPC900 (inset: Pt/C) before and after 1000 CV cycle in O_2-saturated 0.1 M KOH. (b) CV curves for TNPC900 (inset: Pt/C) before and after 3 M methanol addition

Conclusion

We successfully fabricated nitrogen-doped porous carbon from textile waste through chemical activation and pyrolysis. Calcium chloride-induced pore formation and urea served as the nitrogen precursor. Different pyrolysis temperatures (from 800 °C to 1000 °C) impacted the surface characteristics and ORR performance of the TNPCs produced. Among the TNPCs prepared, TNPC900 catalyst exhibited the highest ORR activity with the least H_2O_2 formation. The excellent electrocatalytic activity may be attributed to the collusion of high surface area, proper ratio of mesopores and micropores, and high pyridinic-N. Although ORR performance was slightly inferior to that of Pt/C, TNPC900 is a good potential Pt substitute because of its abundantly available resource and simple production method. TNPC900 also showed better stability and methanol immunity than commercial Pt/C catalyst, making it potentially suitable for direct methanol fuel-cell application.

Acknowledgement

This work is financially supported by the Ministry of Higher Education of Malaysia: TRGS/1/2018/UKM/01/6/2 and Universiti Kebangsaan Malaysia: DIP-2019-021.

References

1. Steele, B. C. H. and Heinzel, A. (2001). Materials for fuel-cell technologies. *Nature*, 414(6861): 345-352.
2. Wang, Y., Li, J. and Wei, Z. (2018). Transition-metal-oxide-based catalysts for the oxygen reduction reaction. *Journal of Materials Chemistry A*, 6(18): 8194-8209.
3. Karim, N. A. and Kamarudin, S. K. (2013). An overview on non-platinum cathode catalysts for direct methanol fuel cell. *Applied Energy*, 103(9): 212-220.
4. Wu, Z., Song, M., Wang, J. and Liu, X. (2018). Recent progress in nitrogen-doped metal-free electrocatalysts for oxygen reduction reaction. *Catalysts*, 8(5): 196.
5. Guo, D., Shibuya, R., Akiba, C., Saji, S., Kondo, T. and Nakamura, J. (2016). Active sites of nitrogen-doped carbon materials for oxygen reduction reaction clarified using model catalysts. *Science*, 351(6271): 361-365.
6. Li, J., Wang, S., Ren, Y., Ren, Z., Qiu, Y. and Yu, J. (2014). Nitrogen-doped activated carbon with micrometer-scale channels derived from luffa sponge fibers as electrocatalysts for oxygen reduction reaction with high stability in acidic media. *Electrochimica Acta*, 149: 56-64.

7. Quílez-Bermejo, J., Morallón, E. and Cazorla-Amorós, D. (2020). Metal-free heteroatom-doped carbon-based catalysts for ORR. A critical assessment about the role of heteroatoms. *Carbon*, 165: 434-454.
8. Gao, Z., Zhang, Y., Song, N. and Li, X. (2017). Biomass-derived renewable carbon materials for electrochemical energy storage. *Materials Research Letters*, 5(2): 69-88.
9. Borghei, M., Lehtonen, J., Liu, L. and Rojas, O. J. (2018). Advanced biomass-derived electrocatalysts for the oxygen reduction reaction. *Advanced Materials*, 30(24): 1703691.
10. Kaur, P., Verma, G. and Sekhon, S. S. (2019). Biomass derived hierarchical porous carbon materials as oxygen reduction reaction electrocatalysts in fuel cells. *Progress in Materials Science*, 102: 1-71.
11. Zhou, H., Zhang, J., Zhu, J., Liu, Z., Zhang, C. and Mu, S. (2016). A self-template and KOH activation co-coupling strategy to synthesize ultrahigh surface area nitrogen-doped porous graphene for oxygen reduction. *RSC Advances*, 6(77): 73292-73300.
12. Zheng, B., Wang, J., Pan, Z., Wang, X., Liu, S., Ding, S. and Lang, L. (2020). An efficient metal-free catalyst derived from waste lotus seedpod for oxygen reduction reaction. *Journal of Porous Materials*, 27(3): 637-646.
13. Polajnar Horvat, K. and Šrimpf Vendramin, K. (2021). Issues surrounding behavior towards discarded textiles and garments in Ljubljana. *Sustainability (Switzerland)*, 13(11): 1-11.
14. USEPA (2019). Textiles: Material-specific data. Available from https://www.epa.gov/facts-and-figures-about-materials-waste-and-recycling/textiles-material-specific-data#TextilesOverview. [Accessed online: 16-Dec-2019].
15. Ramamoorthy, S. K., Skrifvars, M., Alagar, R. and Akhtar, N. (2018). End-of-life textiles as reinforcements in biocomposites. *Journal of Polymers and the Environment*, 26(2): 487-498.
16. Sauid, S. M., Kamarudin, S. K., Karim, N. A. and Shyuan, L. K. (2021). Superior stability and methanol tolerance of a metal-free nitrogen-doped hierarchical porous carbon electrocatalyst derived from textile waste. *Journal of Materials Research and Technology*, 11: 1834-1846.
17. Ge, X., Sumboja, A., Wuu, D., An, T., Li, B., Goh, F. W. T., … and Liu, Z. (2015). Oxygen reduction in alkaline media: from mechanisms to recent advances of catalysts. *ACS Catalysis*, *5*(8): 4643-4667.
18. Ratso, S., Kruusenberg, I., Käärik, M., Kook, M., Saar, R., Kanninen, P., … and Tammeveski, K. (2017). Transition metal-nitrogen co-doped carbide-derived carbon catalysts for oxygen reduction reaction in alkaline direct methanol fuel cell. *Applied Catalysis B: Environmental*, 219: 276-286.
19. Zhou, R., Zheng, Y., Jaroniec, M. and Qiao, S. Z. (2016). Determination of the electron transfer number for the oxygen reduction reaction: From theory to experiment. *ACS Catalysis*, 6(7): 4720-4728.
20. Tang, J., Wang, Y., Zhao, W., Zeng, R. J., Liu, T. and Zhou, S. (2019). Biomass-derived hierarchical honeycomb-like porous carbon tube catalyst for the metal-free oxygen reduction reaction. *Journal of Electroanalytical Chemistry*, 847: 113230.
21. Shi, J., Lin, N., Lin, H. B., Yang, J. and Zhang, W. L. (2020). A N-doped rice husk-based porous carbon as an electrocatalyst for the oxygen reduction reaction. *Xinxing Tan Cailiao/New Carbon Materials*, 35(4): 401-409.
22. Thommes, M., Smarsly, B., Groenewolt, M., Ravikovitch, P. I. and Neimark, A. V. (2006). Adsorption hysteresis of nitrogen and argon in pore networks and characterization of novel micro- and mesoporous silicas. *Langmuir*, 22(2): 756-764.
23. Jiang, M., Yu, X., Yang, H. and Chen, S. (2020). Optimization strategies of preparation of biomass-derived carbon electrocatalyst for boosting oxygen reduction reaction: A minireview. *Catalysts*, 10(12): 1-17.

24. Mao, X., Cao, Z., Yin, Y., Wang, Z., Dong, H. and Yang, S. (2018). Direct synthesis of nitrogen and phosphorus co-doped hierarchical porous carbon networks with biological materials as efficient electrocatalysts for oxygen reduction reaction. *International Journal of Hydrogen Energy*, 43(22): 10341-10350.
25. Zhao, Q., Ma, Q., Pan, F., Wang, Z., Yang, B., Zhang, J. and Zhang, J. (2016). Facile synthesis of nitrogen-doped carbon nanosheets as metal-free catalyst with excellent oxygen reduction performance in alkaline and acidic media. *Journal of Solid State Electrochemistry*, 20(5): 1469-1479.
26. Zhang, W., Qi, J., Bai, P., Wang, H. and Xu, L. (2019). High-level nitrogen-doped, micro/mesoporous carbon as an efficient metal-free electrocatalyst for the oxygen reduction reaction: Optimizing the reaction surface area by a solvent-free mechanochemical method. *New Journal of Chemistry*, 43(27): 10878-10886.
27. Lazar, P., Mach, R. and Otyepka, M. (2019). Spectroscopic fingerprints of graphitic, pyrrolic, pyridinic, and chemisorbed nitrogen in N-doped graphene. *Journal of Physical Chemistry C*, 123(16): 10695-10702.
28. Zainul Abidin, A. F., Loh, K. S., Wong, W. Y. and Mohamad, A. B. (2019). Nitrogen-doped carbon xerogels catalyst for oxygen reduction reaction: Improved structural and catalytic activity by enhancing nitrogen species and cobalt insertion. *International Journal of Hydrogen Energy*, 44(54): 28789-28802.
29. Sharifi, T., Hu, G., Jia, X. and Wågberg, T. (2012). Formation of active sites for oxygen reduction reactions by transformation of nitrogen functionalities in nitrogen-doped carbon nanotubes. *ACS Nano*, 6(10): 8904-8912.
30. Liu, R., Zhang, H., Liu, S., Zhang, X., Wu, T., Ge, X., … and Wang, G. (2016). Shrimp-shell derived carbon nanodots as carbon and nitrogen sources to fabricate three-dimensional N-doped porous carbon electrocatalysts for the oxygen reduction reaction. *Physical Chemistry Chemical Physics*, 18(5): 4095-4101.
31. Zheng, F. Y., Li, R., Ge, S., Xu, W. R. and Zhang, Y. (2020). Nitrogen and phosphorus co-doped carbon networks derived from shrimp shells as an efficient oxygen reduction catalyst for microbial fuel cells. *Journal of Power Sources*, 446: 227356.
32. Lai, L., Potts, J. R., Zhan, D., Wang, L., Poh, C. K., Tang, C. and Ruoff, R. S. (2012). Exploration of the active center structure of nitrogen-doped graphene-based catalysts for oxygen reduction reaction. *Energy and Environmental Science*, *5*(7): 7936-7942.
33. Xu, S. S., Qiu, S. W., Yuan, Z. Y., Ren, T. Z. and Bandosz, T. J. (2019). Nitrogen-containing activated carbon of improved electrochemical performance derived from cotton stalks using indirect chemical activation. *Journal of Colloid and Interface Science*, 540: 285-294.
34. Akula, S. and Sahu, A. K. (2019). Heteroatoms co-doping (N, F) to the porous carbon derived from spent coffee grounds as an effective catalyst for oxygen reduction reaction in polymer electrolyte fuel cells. *Journal of The Electrochemical Society*, 166(2): F93-F101.
35. Li, D., Fan, Y., Yuan, H., Deng, L., Yang, J., Chen, Y. and Luo, B. (2020). Renewable and metal-free carbon derived from aquatic scindapsus affording meso–microporosity, large interface, and enriched pyridinic-N for efficient oxygen reduction reaction catalysis. *Energy & Fuels*, 34(10): 13089-13095.
36. Fan, Z., Li, J., Zhou, Y., Fu, Q., Yang, W., Zhu, X. and Liao, Q. (2017). A green, cheap, high-performance carbonaceous catalyst derived from *Chlorella pyrenoidosa* for oxygen reduction reaction in microbial fuel cells. *International Journal of Hydrogen Energy*, 42(45): 27657-27665.
37. Cao, C., Wei, L., Zhai, Q., Wang, G. and Shen, J. (2017). Biomass-derived nitrogen and boron dual-doped hollow carbon tube as cost-effective and stable synergistic catalyst for oxygen electroreduction. *Electrochimica Acta*, 249: 328-336.